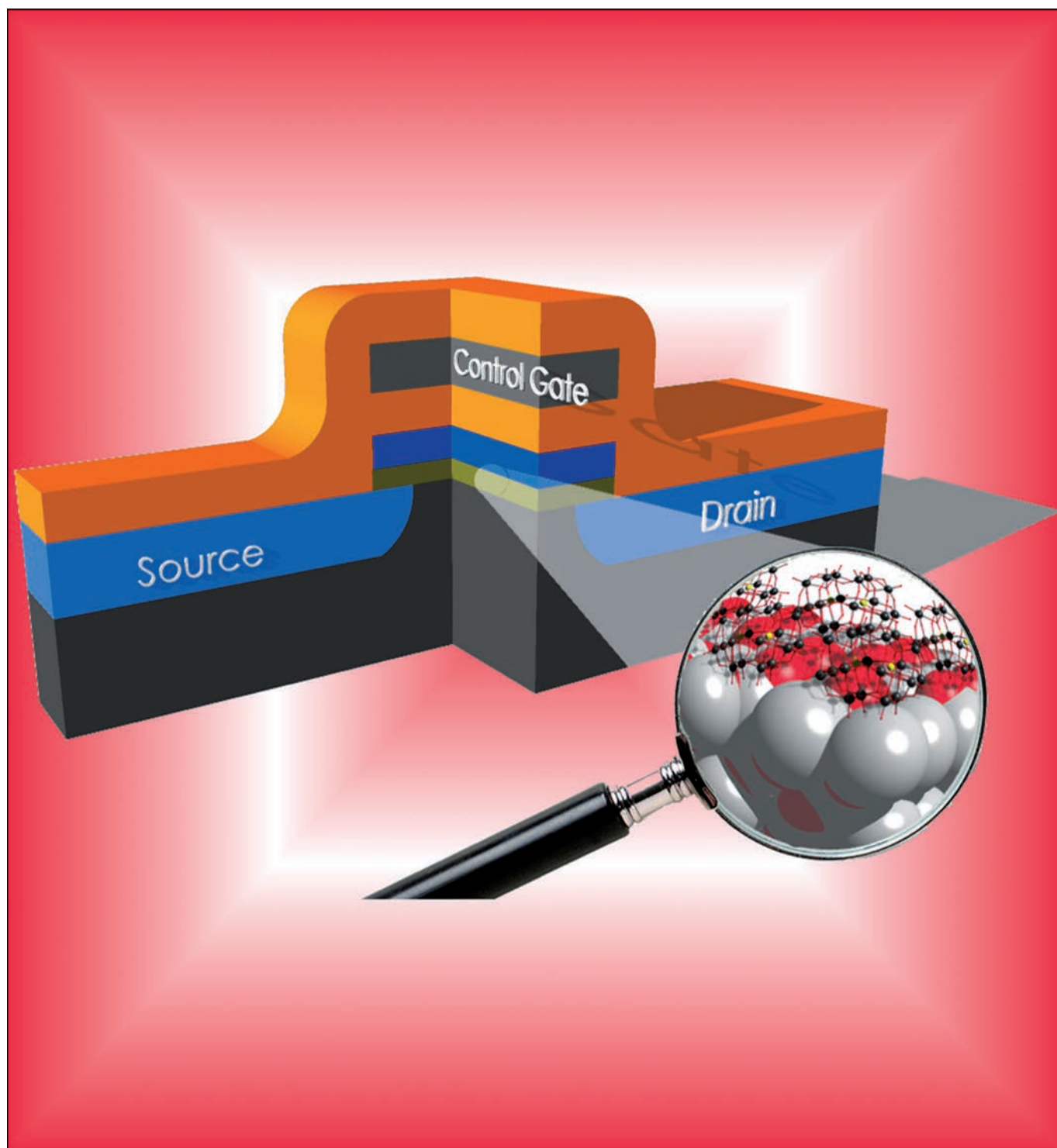


## Towards Polyoxometalate-Cluster-Based Nano-Electronics

Laila Vilà-Nadal,<sup>[a]</sup> Scott G. Mitchell,<sup>[a]</sup> Stanislav Markov,<sup>[b]</sup> Christoph Busche,<sup>[a]</sup>  
Vihar Georgiev,<sup>[b]</sup> Asen Asenov,<sup>[b]</sup> and Leroy Cronin\*<sup>[a]</sup>



**Abstract:** We explore the concept that the incorporation of polyoxometalates (POMs) into complementary metal oxide semiconductor (CMOS) technologies could offer a fundamentally better way to design and engineer new types of data storage devices, due to the enhanced electronic complementarity with SiO<sub>2</sub>, high redox potentials, and multiple redox states accessible to polyoxometalate clusters. To explore this we constructed a custom-built simulation domain bridge. Connecting DFT, for the quantum mechanical modelling part, and mesoscopic device modelling, confirms the theoretical basis for the proposed advantages of POMs in non-volatile molecular memories (NVMM) or flash-RAM.

**Keywords:** nanoelectronics · nanosystems · polyoxometalates · redox-active systems

## Introduction

Polyoxometalates (POMs) are discrete metal-oxide clusters formed from early transition-metal ions and oxo ligands. POMs constitute a distinct fundamental category of compounds, offering value and potential for both theoretical and practical applications.<sup>[1]</sup> The first known POM, the phosphomolybdate [PMo<sub>12</sub>O<sub>40</sub>]<sup>3-</sup>, was reported in 1826 by Berzelius,<sup>[2]</sup> and in 1864 Marignac observed two isomers, now designated by  $\alpha$  and  $\beta$ , of the silicotungstic acid [SiW<sub>12</sub>O<sub>40</sub>]<sup>4-</sup>.<sup>[3]</sup> Historically, the polyoxoanions of Mo<sup>VI</sup> and W<sup>VI</sup> have been the predominant species. Hundreds, if not thousands, of such complexes have been synthesized to date, and this extraordinarily rich field is far from exhausted. POMs have been used as valuable industrial catalysts,<sup>[4]</sup> they also have a very rich electrochemistry offering a wide range of controllable reduction potentials.<sup>[5]</sup> Furthermore, POMs are useful as specialized oxidizing agents<sup>[6]</sup> and they have a notable potential in areas such as photochemistry,<sup>[7]</sup> photocatalysis,<sup>[8]</sup> medicine,<sup>[4]</sup> and magnetism<sup>[9a]</sup> including exciting possibilities for the development of POM-based QBITS.<sup>[9b]</sup> Consequently, POM chemistry is a key emerging area that promises to allow the development of sophisticated designer molecule-based materials and devices that exploit develop-

ments in instrumentation and nanoscale science with emerging material fabrication methods.<sup>[10]</sup>

The conventional Wells–Dawson 18 metal ion of general formula [M<sub>18</sub>O<sub>54</sub>(XO<sub>4</sub>)<sub>2</sub>]<sup>m-</sup> (M=Mo, W; X=P, As, S)<sup>[11,12]</sup> is one of the most studied clusters, since the structure of [W<sub>18</sub>O<sub>54</sub>(PO<sub>4</sub>)<sub>2</sub>]<sup>6-</sup> was resolved more than 50 years ago.<sup>[10]</sup> Their elliptical shape encapsulates two ‘load-bearing’ tetrahedral anions such as sulfate [S<sup>VI</sup>O<sub>4</sub>]<sup>2-</sup> or phosphate [P<sup>V</sup>O<sub>4</sub>]<sup>3-</sup>, which are vital for retaining the structural integrity of the cluster, but are normally chemically inert.<sup>[13]</sup> In fact, there are a few examples of Wells–Dawson clusters hosting non-tetrahedral anions: [BiO<sub>3</sub>]<sup>3-</sup>, [AsO<sub>3</sub>]<sup>3-</sup>, [P<sub>2</sub>O<sub>7</sub>]<sup>4-</sup>.<sup>[14]</sup> Our group’s interest in developing new non-conventional Wells–Dawson clusters has resulted in a synthetic strategy to encapsulate two pyramidal sulfite ions [SO<sub>3</sub>]<sup>2-</sup>,<sup>[12,15]</sup> or one central [TeO<sub>6</sub>]<sup>6-</sup>,<sup>[16]</sup> [IO<sub>6</sub>]<sup>5-</sup>,<sup>[17]</sup> or [WO<sub>6</sub>]<sup>6-</sup> anion.<sup>[18]</sup> Apart from the synthetic challenge, the incorporation of electronically active templates in the Wells–Dawson cluster opens the way to the design of molecular devices exhibiting properties not observed in their bulk analogues: for example, allowing the engineering of single-molecule electronic devices.<sup>[19]</sup> The idea of molecular electronics was first postulated in 1973 when Aviram and Ratner speculated about organic molecules as components in electronic circuits.<sup>[20]</sup> Since then, the emerging field of molecular electronics typically utilizes switchable organic molecules anchored between nano-electrodes, such as molecular memory arrays based on rotaxanes, which demonstrate the first molecular-based RAM.<sup>[21]</sup> From an engineering perspective, however, organic molecular electronics raises questions of high resistance and power, low performance and problematic fabrication, reproducibility and reliability: our strategy is to resolve these issues by using molecules that are better-matched to their substrate.<sup>[17]</sup> POMs offer a fundamentally better electronic complementarity with SiO<sub>2</sub> than organic molecules due to their oxidic nature.

In this Concept article we propose the use of polyoxometalates as nanoscale molecular memory elements. As such this Concept article builds on and extends our previous concept article, published in this journal in 2006,<sup>[23]</sup> which postulated that polyoxometalate clusters, due to their nanoscale size and novel electronic properties, could play an important role in the development of polyoxometalate integrated nanosystems.

Furthermore, they are highly redox active and can be doped with electronically active heteroatoms. The electronic and structural properties of the Wells–Dawson class, see Figure 1, offer an inviting avenue for their application in non-volatile molecular memories (NVMM). We first elaborate on the rationale behind this vision and present the first flash cell modeling evaluation of POMs in the context of operation and statistical variability in NVMM.

The ideas and results presented herein focus on non-volatile molecular memories, in which the logical state of the memory cell is determined by the amount of net charge, or

[a] Dr. L. Vilà-Nadal, Dr. S. G. Mitchell, Dr. C. Busche, Prof. L. Cronin  
WestCHEM, School of Chemistry  
Joseph Black Building, University of Glasgow  
University Avenue, Glasgow, G12 8QQ (UK)  
Fax: (+44)141-330-4888  
E-mail: L.Cronin@chem.gla.ac.uk

[b] Dr. S. Markov, Dr. V. Georgiev, Prof. A. Asenov  
Department of Electronics & Electrical Engineering  
Rankine Building, University of Glasgow  
Oakfield Avenue, Glasgow, G12 8QQ (UK)

Supporting information for this article is available on the WWW under <http://dx.doi.org/10.1002/chem.201301631>.

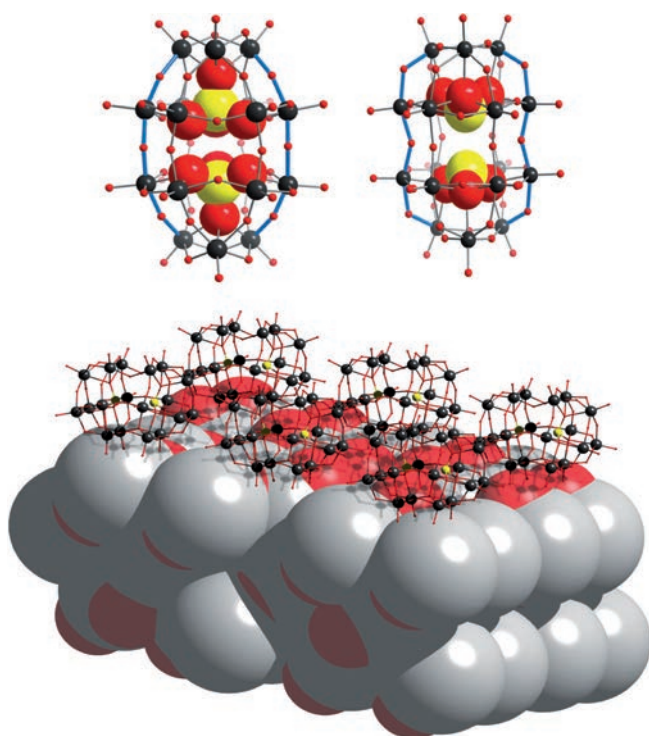


Figure 1. Top left: Ball-and-stick view of the classic Wells–Dawson structure  $[M_{18}O_{54}(SO_4)_2]^{4-}$   $M=W$  and  $Mo$ . Top right: Ball-and-stick view of the non-classical Wells–Dawson anion  $[M_{18}O_{54}(SO_3)_2]^{4-}$  for  $M=W$  and  $Mo$ . Bottom: idealised vision of a POM layer on  $SiO_2$ . Colour code for spheres and wires:  $M=black$ ,  $O=red$ ,  $S=yellow$ ,  $Si=grey$ , blue colour for  $M-O-M$  bonds is used to highlight the shape of both structures: cylinder- and hourglass-shaped, respectively.

the charge polarisation, in a layer of molecules in a particular reduction/oxidation state. This charge embedded in the gate dielectric controls the threshold voltage, the conductivity of a transistor channel. The readout signal is the change in channel-current that corresponds to a change in the redox state of the molecules, as schematically illustrated in Figure 2. Indeed, this is the concept of the SONOS (silicon-oxide-nitride-oxide-silicon) floating-gate memories,<sup>[24]</sup> except for the nitride charge-trapping layer being replaced by the molecular layer.

The use of redox-active molecules to form the floating gate offers several very important advantages over the conventional polysilicon floating gate,<sup>[24]</sup> or alternatives like trap-rich dielectrics (e.g.  $Si_3N_4$ )<sup>[25]</sup> or metallic nano-clusters.<sup>[26]</sup> In particular, the charge storage is very localised, thus minimising cross-cell capacitive coupling (arising from charge redistribution on the sides of a poly-Si floating gate, and being one of the most critical issues with flash memories). Although this benefit is present in floating gates realised by charge-trapping dielectric or by a metallic nano-cluster array, both technologies exhibit very large variability—charge-trap memories suffer variation in trap-density and trap-energy,<sup>[27]</sup> and the size and density of nano-clusters is difficult to control—which precludes their ultimate miniaturisation.<sup>[28]</sup>

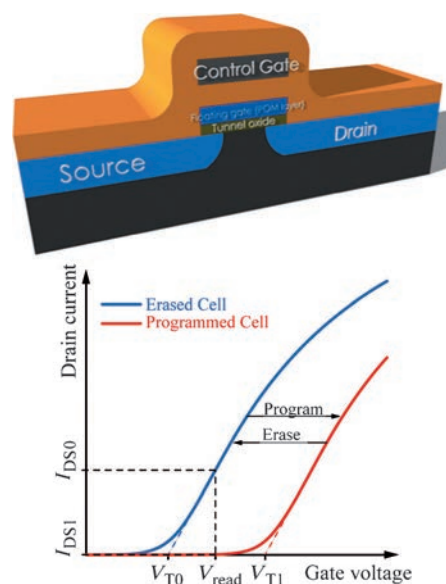


Figure 2. Top: Schematic representation of a single-transistor non-volatile memory cell, indicating the aimed substitution of the poly-Si floating gate with an array of polyoxometalate clusters (POM layer), pursuing further miniaturisation of the memory cell into the few-nm linear dimension. Bottom: Transfer characteristics (source-drain current versus the control gate bias) of the device, illustrating the effect of reducing (programming) the POM layer, leading to a reduction of the current in the semi-conductive channel between the source and drain. The magnitude of the source-drain current at a given bias of the control gate represents the readout signal, hence the logic state—it is modulated by the presence or absence of charge stored in the floating gate.

Chemical synthesis in combination with molecular self-assembly of redox-active molecules can yield a very regular distribution (spatially, and energetically) of charge-storage centres,<sup>[29]</sup> and thus allow scaling of the floating gate down to a few nanometres. In fact, this concept has already been demonstrated for organic redox-active molecules.<sup>[30]</sup> However, a major issue in this case is the low retention time, due to the small redox potentials associated with the organic redox-active molecules (e.g. ferrocene, and porphyrin). In this respect, the Wells–Dawson POM class may be perfect, possessing much better stability and substantially higher redox potentials. Additionally, POMs exhibit multiple redox states (e.g. can be multiply reduced)—an essential feature that can be used as a safeguard against variability, or to realise a multi-bit storage cell. Finally, the chemistry of the POMs, being oxygen-rich clusters (molecular metal oxides), would translate in better integration with the standard gate-stack materials and processing used in contemporary flash-memory technology. In fact we have shown a new strategy for the formation of POM architectures on surfaces, using a symmetric amphiphilic Mn-Anderson POM. This system exhibits a fascinating 2-D self-assembly in micrometric hexagonal structures and acts as effective smart nanodielectric material.<sup>[31]</sup>

In the present Concept article we have selected a nano-scale molecular cluster with a  $\{M_{18}^{VI}O_{54}\}$  ( $M=W, Mo$ ) shell to encapsulate charge-bearing anions, which has an interior

cavity large enough to include two active sulfite  $[\text{S}^{\text{IV}}\text{O}_3]^{2-}$  ions or two inert sulfate  $[\text{S}^{\text{VI}}\text{O}_4]^{2-}$  ions (see Figure 1). Both anions are electronically interesting, especially  $[\text{S}^{\text{IV}}\text{O}_3]^{2-}$  because the sulfur atoms are in an intermediate oxidation state and possess a vacant coordination site, a lone pair of electrons, and can change oxidation state and coordination number; in contrast to  $[\text{SO}_4]^{2-}$  which is not redox active. We start by presenting the electronic structure description of the clusters by means of DFT calculations and, as a final point, we present a new methodology that allows the simulation of POMs integrated into a flash-cell memory.

### Electronic Structure of $[\text{M}_{18}\text{O}_{54}(\text{SO}_4)_2]^{4-}$ and $[\text{M}_{18}\text{O}_{54}(\text{SO}_3)_2]^{4-}$ for $\text{M} = \text{W}$ and $\text{Mo}$

One of the fundamental challenges faced by researchers is the interpretation of the electrochemical data: cyclic voltammetry provides an unambiguous indicator of a redox event, but not its localisation within the molecule. By incorporating an appropriate solvent model, we will compute ab initio the redox potentials of known and unknown species, the aim being to identify species such that might be influenced by an appropriate gate potential. Our preliminary work on the bisulfite clusters shows that the reorganisation of charge can be triggered by supporting the cluster on a gold surface, the mirror charges below the surface provide an electric field gradient that draws the electron density into the conduction band.<sup>[13]</sup> This naturally poses the question: how would the molecules behave under an applied voltage. The calculations described in this section aim to address one simple question: are appropriately substituted POMs competent to perform the electronic tasks (i.e. conduction and rectification) that would make them viable components of a flash memory cell? This is important since POMs are *easily reducible* chemical species and are often referred to as a *reservoir* of electrons.

POMs in their fully oxidised state are structurally stable in the solid state as well as in solution, in the presence of counteranions to balance their negative charge. In general, the highest occupied molecular orbitals are oxygen p-like (oxo band), and the set of lowest unoccupied orbitals are metal d-like (metal band),<sup>[32]</sup> thus we frequently use the terms *oxo band* and *metal band of unoccupied orbitals*, respectively. It is worth noting though that these sets of orbitals do not form a band in the strict sense, since the orbital energy is separated by discrete energies in these medium-sized clusters.<sup>[33]</sup> In the classic Wells–Dawson clusters (cylinder-shaped) the HOMO is mainly delocalised over oxygen atoms (see Figure 3), whereas for the non-classic clusters (hourglass-shaped) it is delocalised over the  $[\text{SO}_3]^{2-}$  moiety; the subsequent molecular orbitals (LUMO) belong to the equatorial metals in both cases. So, in both cases the LUMO is delocalised over metal centres that are connected to each other by large M–O–M angles,<sup>[34]</sup> with values ranging from approximately  $145^\circ$  to  $165^\circ$ , see Table 1 for details. Table 1 presents the values for the HOMO and LUMO orbitals of

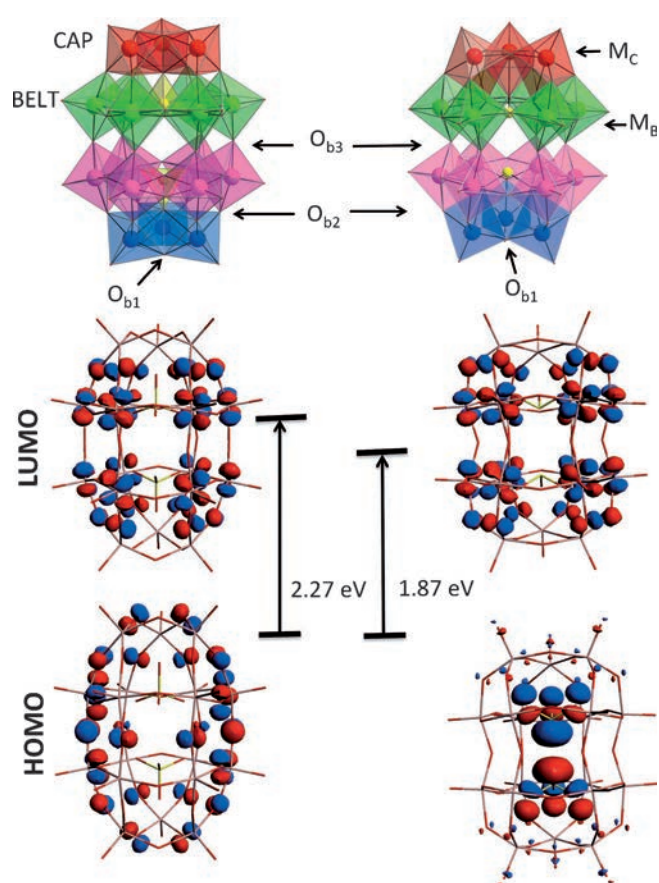


Figure 3. Top-Left: polyhedral representation of the  $\alpha$ - $[\text{X}_2\text{W}_{18}\text{O}_{62}]^{n-}$  classic Wells–Dawson anion. Top-Right: polyhedral representation of the  $\alpha$ - $[\text{X}_2\text{W}_{18}\text{O}_{60}]^{n-}$  non-classic Wells–Dawson anion. Two identical fragments or hemispheres are easily identifiable, each composed of one  $[\text{M}_3\text{O}_6]$  triad (red and blue, named CAP) and one  $[\text{M}_6\text{O}_{18}]$  equatorial belt with six  $\text{WO}_6$  octahedra (green and purple, named BELT). In both cases X = heteroatom units are represented in yellow. Relevant positions are labelled for further discussion. Bottom: Graphical representation comparing the HOMO–LUMO gap in eV for the classical  $[\text{W}_{18}\text{O}_{54}(\text{SO}_4)_2]^{4-}$  (left) and the non-classical (right) Wells–Dawson anion  $[\text{W}_{18}\text{O}_{54}(\text{SO}_3)_2]^{4-}$ .

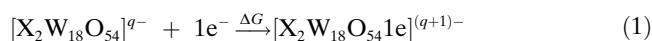
the optimized classical  $[\text{M}_{18}\text{O}_{54}(\text{SO}_4)_2]^{4-}$  and the non-classical  $[\text{M}_{18}\text{O}_{54}(\text{SO}_3)_2]^{4-}$  Wells–Dawson anions, for  $\text{M} = \text{W}$ ,  $\text{Mo}$ . In Wells–Dawson-like clusters, the first reduction occurs in the equatorial (belt) region. The reduction of the cluster does not change the net charge on the internal heteroatom since the additional electrons go to addenda symmetry-adapted orbitals.<sup>[41]</sup> The energy of the lowest unoccupied orbitals must be low enough to accept the incoming electron. The crystal field in the solid state and the solvent molecules in dilute solutions stabilise the anion, placing the molecular orbitals at the appropriate level.<sup>[35]</sup> In fact, the redox properties of a POM are closely related to the relative energy and composition of the LUMO. As depicted in Figure 3, the metallic orbitals in  $[\text{W}_{18}\text{O}_{54}(\text{SO}_4)_2]^{4-}$  and  $[\text{W}_{18}\text{O}_{54}(\text{SO}_3)_2]^{4-}$  have both antibonding character between the metal and oxygen orbitals but also between two adjacent metals. We have calculated tungsten clusters under  $D_{3h}$  and molybdenum clusters under  $D_{3h}$  and  $D_3$  symmetry constraints. Previ-

Table 1. Orbital energies (in eV), experimental ( $E_{1/2}$ ), theoretical ( $E_c$ ) absolute values for the first cathodic peaks (in V) and relevant theoretical interatomic distances (in Å) and angles (in °) for the COSMO-optimised classical  $[M_{18}O_{54}(SO_4)_2]^{4-}$   $M=W, Mo$  and the non-classical Wells–Dawson anion  $[M_{18}O_{54}(SO_3)_2]^{4-}$   $M=W, Mo$ . Molybdenum compounds are optimized for  $D_{3h}$  and  $D_3$  symmetry. RE = reduction energy.

M	$X_2$	Sym	Relevant distances and angles <sup>[a]</sup>				$E_{HOMO}$	$E_{LUMO}$	$\Delta E_{H-L}$ <sup>[b]</sup>	$E_{1/2}$ vs. (Fc <sup>+</sup> /Fc)	RE (eV)	$E_c$ vs. (NHE) <sup>[c]</sup>	$\Delta(E_{1/2}-E_c)$ <sup>[d]</sup>
			M <sub>C</sub> -O <sub>b1</sub>	M <sub>C</sub> -O <sub>b2</sub>	M <sub>B</sub> -O <sub>b3</sub>	M <sub>B</sub> -O <sub>b3</sub> -M <sub>B</sub>							
W	SO <sub>4</sub> <sup>2-</sup>	$D_{3h}$	1.94 (1.91) <sup>[e]</sup>	1.92 (1.89)	1.92 (1.89)	164.61 (161.19)	-6.89	-4.62	2.27	-0.27 <sup>[j]</sup>	-4.44	-4.64	0.20
W	SO <sub>3</sub> <sup>2-</sup>	$D_{3h}$	1.92 (1.89) <sup>[f]</sup>	1.93 (1.93)	1.92 (1.92)	147.55 (145.58)	-6.48	-4.61	1.87	-0.35 <sup>[j]</sup>	-4.37	-4.55	0.18
Mo	SO <sub>4</sub> <sup>2-</sup>	$D_{3h}$	1.94 (1.93) <sup>[g]</sup>	1.92 (1.87)	1.92 (1.87)	164.44 (164.58)	-6.77	-5.15	1.62	-0.10 <sup>[k]</sup>	-5.08	-4.81	0.27
		$D_3$	1.87	1.93	1.94	164.78	-6.80	-5.07	1.73		-5.04	-4.81	0.23
Mo	SO <sub>3</sub> <sup>2-</sup>	$D_{3h}$	1.93 (1.96) <sup>[h]</sup>	1.94 (1.81)	1.94 (1.92)	146.94 (145.79)	-6.06	-5.18	0.88	-0.01 <sup>[l]</sup>	-5.10	-4.90	0.19
		$D_3$	1.94	1.95	1.95	147.97	-6.18	-5.06	1.12		-5.00	-4.90	0.09

[a] See Figure 3 for notation of metal and oxygen sites, averaged experimental values in parentheses. [b]  $\Delta E_{H-L} = E_{LUMO} - E_{HOMO}$  (eV). [c] Predicted absolute potential versus NHE using Cramer corrected *absolute zero potential*. [d] Difference between computed and experimental potentials. [e] Ref. [35]. [f] Ref. [15c]. [g] Ref. [36]. [h] Ref. [37]. [i] Ref. [38]. [j] Ref. [12]. [k] Ref. [40]. [l] Ref. [41].

ous studies have demonstrated that alternating short and long bond length distortions are particularly pronounced in the molybdates relative to the tungstates and exert influence on POM reduction potentials.<sup>[43]</sup> In fact, reduction potentials may be estimated theoretically by calculating the fully oxidised molecule and its one-electron reduced partner.<sup>[32]</sup> We can theoretically estimate the redox potential of a given POM by determining the free energy associated with the process [Eq. (1)].



The reduction process of a POM involves the addition of one electron to an almost nonbonding orbital, thus the entropic and vibrational contributions to  $\Delta G$  in Equation (1) can be replaced by its electronic contribution in solution, the reduction energy.<sup>[31]</sup> In the present study, the reduction energy is defined as the energy difference between the one-electron reduced and the oxidized forms of the Wells–Dawson anion. Because the anion charges of the reduced and oxidized forms differ, the reduction energy must be computed in the presence of a solvent model (conductor-like screening model (COSMO)).<sup>[45]</sup> Otherwise, energies would not be reliable for comparison with experimental values.<sup>[35]</sup> As in electrochemical data in which the normal hydrogen electrode (NHE) is taken as the zero on the relative scale, the theoretical values need to be referred to an absolute theoretical zero. Cramer et al. have recently recalculated this absolute zero to be 4.28 eV for the free energy change in the NHE reaction:  $\frac{1}{2} H_2 \rightarrow H^+ + e^-$ .<sup>[46]</sup>

Table 1 summarises the first one-electron reduction energies for the four clusters studied here and their relationship with the experimental first reduction peaks. Half-wave potentials versus NHE and theoretical estimates of the reduction energy are shown in the last columns. We have determined the cathodic peaks ( $E_c$ ) for Dawson clusters using the equation  $E^\circ = -\Delta G^\circ/nF$  and the Cramer value 4.28 eV. As shown in the last column in Table 1, we have found small discrepancies between the theoretical and the experimental slopes. Reduction energies are more negative (more favourable) for molybdenum clusters and their theoretical values are in good agreement with experimental ones. The experi-

mental structure of Mo clusters is better reproduced with calculations carried out with  $D_3$  symmetry, their reduction energy values are also slightly improved. Lowering the symmetry from  $D_{3h}$  to  $D_3$  also has a great impact in the value of the H–L gap, see for instance  $[Mo_{18}O_{54}(SO_3)_2]^{4-}$  its H–L gap is enlarged from 0.88 to 1.12 eV.

## The Flash Cell Modelling

**Flash cell design:** To evaluate the suitability of Wells–Dawson clusters for the realization of the floating gate in a non-volatile molecular memory material, we developed a simulation flow that links density functional theory (DFT) results to three-dimensional (3D) numerical flash cell simulations. The simplified block diagram is illustrated in Figure 4. Central to this flow is the custom-built *simulation domain bridge*, connecting the two distinct modelling domains—DFT, for the molecular part, and mesoscopic device modelling. An n-channel flash memory cell with an 18 nm by 18 nm square gate has been designed for this study. It is based on a previously studied template 18 nm transistor,<sup>[47]</sup> and is similar to the contemporary flash-cell studied by other authors.<sup>[48]</sup>

It is important to mention that the average acceptor doping in the channel of the transistor is approximately  $5 \times 10^{18} \text{ cm}^{-3}$ . The high level of doping is necessary to maintain good electrostatic integrity at this ultra-short channel length. Alternatively, the impact of the charge stored in the floating gate on the channel potential (hence drain current) will be reduced by the drain bias, even if the bias is low. The gate dielectric (assumed to be hafnium with a dielectric constant of 20.8) is 4 nm thick (distance from substrate to the control gate), and the POM layer is 1.5 nm above the Si substrate. Note that a larger distance between the control gate and the floating gate increases the impact of the charge stored in the latter, but degrades the electrostatic integrity. In fact, optimisation of the gate stack must be done also with regards to the program/erase and retention characteristics of the memory cell, but this is beyond the scope of this study. Here we consider a tunnel oxide scaled to the limit, as projected for charge-trapping memories,<sup>[49]</sup> based on the fact that the

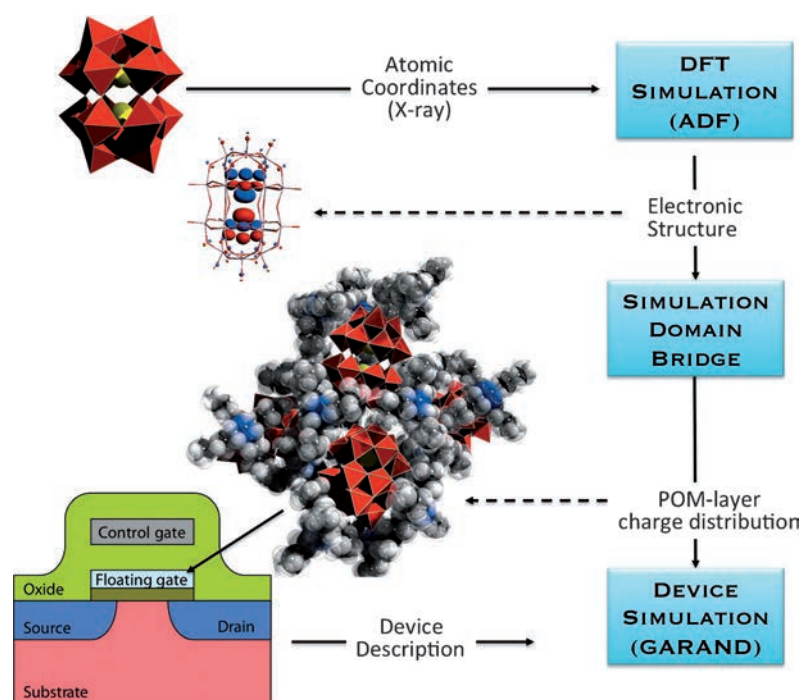


Figure 4. Simplified block diagram of the simulation methodology, linking DFT and flash-cell modelling. The simulation domain bridge is developed in-house. The commercial program simulators ADF and Garand are used for DFT and three-dimensional device simulations, respectively.

reduction energies of all POMs shown in Table 1 lie below the conduction band of the Si substrate ( $-4.05$  eV), hence suggesting sufficient retention. All simulations are performed on a device with a square gate ( $W/L=1$ ) and at low drain bias ( $V_{DS}=50$  mV).

### Simulation Results

Taking the  $[W_{18}O_{54}(SO_3)_2]^{4-}$  POM as an example, in Figure 5 we show the impact of consecutively reducing the clusters in the POM layer by one and by two electrons on

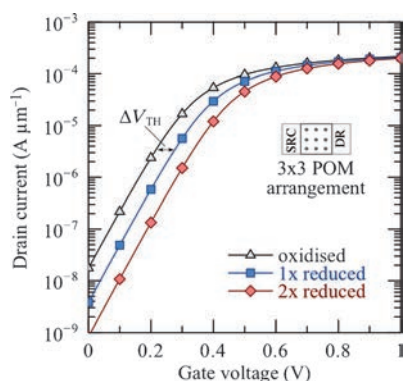


Figure 5. Clear lowering of the source-drain current (sub-threshold region, indicating also threshold voltage shift  $\Delta V_{TH}$ ) corresponding to the reduction of each POM simultaneously by one (blue) and two (red) electrons. Nine POMs in a  $3 \times 3$  matrix comprise the floating gate, as illustrated; the centres of all POMs are  $1.5$  nm above the substrate.

the drain current of the flash memory cell. The POM layer consists of nine clusters, centrally arranged in a regular three-by-three array. The centre of each POM is located  $1.5$  nm above the Si-substrate. The assumption is that all POMs within the layer are simultaneously reduced by one or two electrons. Reducing the POMs adds negative charge to the floating gate, which thus repels electrons from the channel of the transistor. This in turn reduces the drain current, clearly evident in the sub-threshold region (linear part of the semi-log plot in Figure 5), which is directly influenced by the electron density distribution in the channel of the transistor. The simulations performed with different POMs from Table 1 do not yield appreciable difference in the transfer characteristics of the cell, which is explained by

the relatively high-symmetry of the Wells–Dawson POMs leading to a similar charge distribution over all atoms,<sup>[50]</sup> and fast decaying electrostatic potential outside the anions in the device modelling result. This means that from the perspective of chemical synthesis, a relevant constraint is the reduction energies of the first few oxidation states to lie below the Si conduction band of  $-4.05$  eV.

To obtain a quantitative measure of the impact of the oxide charge on the flash-cell characteristics, we consider the shift in threshold voltage  $\Delta V_{TH}$  (i.e. the increase in  $V_{TH}$ ), when POMs are reduced. The threshold voltage is defined in the sub-threshold region of the  $I_D V_G$  characteristics, as the gate voltage  $V_G$ , needed to obtain drain current  $I_D$  of  $2 \mu A \mu m^{-1}$ . The threshold voltage shift is illustrated in Figure 5.

Figure 6 shows the increase in threshold voltage,  $\Delta V_{TH}$ , as a function of the sheet-charge density (normalised by the electron charge  $-q = -1.6 \times 10^{-19}$  C). The line represents the analytical dependence relating a uniform sheet-charge density  $-qN_s$  placed at a distance  $z$  away from the Si/oxide interface in an oxide of thickness  $t_{OX}$ :  $\Delta V_{TH} = qN_s(t_{OX} - z)/\epsilon_{OX}$ , where  $\epsilon_{OX}$  is the permittivity of the oxide. As mentioned in the previous section,  $t_{OX} = 4$  nm,  $z = 1.5$  nm, and  $\epsilon_{OX} = 20.8\epsilon_0$ .<sup>[51]</sup>

The symbols in Figure 6 correspond to the 3D flash-cell simulations for the different lateral configuration of POMs, as indicated schematically in the legend. POMs represented by filled circles reside  $1.5$  nm above the Si-substrate (e.g.,  $z = 1.5$  nm), whereas the POMs represented by empty circles are placed  $3$  nm above the Si. The increase of sheet charge

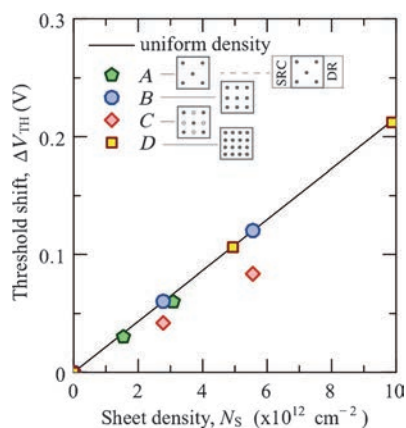


Figure 6. Comparison of the threshold voltage shift  $\Delta V_{TH}$  due to idealised sheet charge in the oxide (line), and due to a POM floating gate (symbols), versus sheet charge density (normalised by the electron charge). The different lateral configurations of the POMs are schematically illustrated. POMs represented by filled circles reside 1.5 nm above the Si-body; POMs represented by empty circles are 3 nm above the Si Body. Therefore in configuration C four of the POMs have reduced impact on the potential and electron density in the channel of the transistor, hence on  $\Delta V_{TH}$ .

density  $N_S$  for a given configuration is achieved by simultaneously reducing the POMs twice. Two important observations can be made in Figure 6. First, for a mono-layer arrangement and regular lateral distribution of POMs,  $\Delta V_{TH}$  agrees well with the idealised analytical model. Moreover, reducing each POM by two electrons produces the same impact on  $V_{TH}$  as doubling the sheet density in the analytical dependence. Therefore, multi-bit storage could be realised with the help of a POM floating gate. The second observation is that a deviation of the POM distribution from a mono-layer has a significant impact on  $\Delta V_{TH}$  and therefore on the readout signal.

The results of Figure 6 are easily understood by comparing the potential barrier profiles along the channel of the

transistor, for the three configurations studied. These are presented in Figure 7, which shows the surface potential barrier as an elevated 2D plot. Since the simulation conditions are the same in each case ( $V_{ds}=50 \text{ mV}$  and  $V_{gs}=0.6 \text{ V}$ ;  $V_{ds}$  and  $V_{gs}$  are the standard notations for the drain-source voltage and gate-source voltage, respectively), the relative height of the barrier is indicative of the relative change in the drain current  $I_D$  (hence  $V_{TH}$ ).

Overall, the barrier is highest for the flat configuration of nine POMs in a  $3 \times 3$  matrix (configuration B), and lowest for the five-POM configuration (A). This is expected since configuration A corresponds to a lower surface charge density, hence a relatively larger number of electrons are induced in the channel. However, configuration C corresponds to the same surface number density as configuration B and still has lower  $V_{TH}$ . This is because four of the POMs, being more distant from the Si-substrate, have substantially reduced impact on the potential and electron density in the channel, as can be easily understood from the relation between  $\Delta V_{TH}$  and  $z$ , mentioned earlier. The reduced impact is clearly seen both in the 2D surface plot and in the equi-potential contour lines.

While this aspect of the simulation results indicates a clear sensitivity to statistical variability in the redox state and spatial distribution of the POMs, Figure 6 also suggests the advantage of POMs being multiply reducible. In particular, the  $\Delta V_{TH}$  value for the five POMs in configuration A, reduced twice, almost equals the  $\Delta V_{TH}$  value due to the nine POMs in configuration C, reduced once. Therefore the multiple-reducibility of the POMs enables the use of an incremental-step-pulse programming (ISPP) algorithm,<sup>[52]</sup> to overcome statistical variability. Nevertheless, the variability arising from the POM layer should also be addressed at the level of POM-layer synthesis. For example, the realisation of inter-POM distances below 1.5 nm, to allow for efficient hopping of electrons between POMs during programming, will provide not only for a higher density of storage centres,

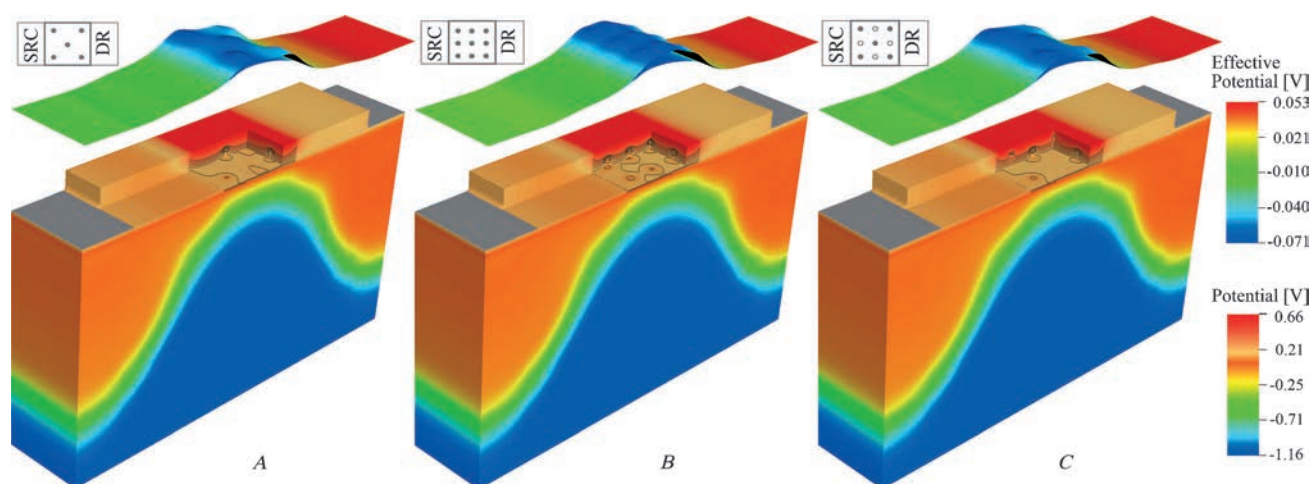


Figure 7. Potential barrier profile along the channel of the flash-cell (2D elevated plot) and distribution of the electrostatic potential of the simulated device (3D); a part from the tunnel oxide is cut away, exposing the local modulation of the potential, due to the charge stored in the nine POMs that form the floating gate. The three different cases correspond to the three configurations from Figure 6, as schematically illustrated.

but also for a more even distribution of the oxidation state between POMs. It may further help in constraining the dispersion in the distance  $z$  between the POMs and the Si substrate.

Finally, we point out that for known bounds of the vertical position of the POMs,  $z$ , one may deploy appropriately thicker tunnel and control oxides to minimize the variability arising from the POM-layer, with the additional benefit of increasing the retention time of the memory cell. However, such increase will lead to undesirable increase in the cell variability arising from random-dopant-fluctuations (RDF) and being proportional to  $t_{\text{OX}}$ .<sup>[53]</sup> The presented modelling framework enables the search for the optimal oxide thicknesses in an engineering context. Our preliminary results in this direction indicate that for a well-optimised 18 nm flash cell, the POM-induced variability could be as low as 20% of the total variability of the cell.

## Summary and Outlook

As is well established, Wells–Dawson POMs can undergo multiple reduction steps under the influence of an applied electric field, accepting more than one electron, without dramatic changes to their geometry. Moreover, it has been shown that the process is reversible—POMs can be brought back to their initial redox-state by applying a field in the opposite direction. This property presents an opportunity for their use as charge-storage centres of a multi-bit memory cell. Here we have established a simulation methodology that goes beyond the modelling of individual POM clusters, and allows us to evaluate their potential as a floating gate in non-volatile memories.

We considered four Wells–Dawson clusters— $[\text{X}_2\text{M}_{18}\text{O}_{54}]^{4-}$ , where M is W or Mo, and X is  $[\text{SO}_4]^{2-}$  or  $[\text{SO}_3]^{2-}$ —the electronic structure of which is well known and their reduction potentials can be understood from both experimental and theoretical points of view. These Wells–Dawson anions appear promising candidates to be incorporated as a floating gate in a non-volatile memory cell. In particular, their small size (ca. 1 nm), and multiple reducibility in a reversible manner, allow for highly localised charge storage. From a device perspective, this means the provision of a mono-disperse energy level (the LUMO) within the band-gap of the gate dielectric, even at relatively high number-density of integrated POMs (ca.  $10^{13} \text{ cm}^{-3}$ ). Indeed, our hierarchical device simulations, incorporating the output of DFT simulations in a model memory cell, confirm the viability of a POM-floating gate in a multi-bit memory. Specifically, we show that the first and second reductions of the clusters in the gate dielectric impart distinct reductions in the drain current, and thus manifest changes in the logic state of the memory cell.

The hierarchical modelling framework permits the exploration of one of the major issues with non-volatile memory miniaturisation—statistical variability. We demonstrate that a variation in the number and spatial configuration of the

POM-floating gate can compromise the readout signal and hence the determination of the logic state, if multi-bit storage per cell is aimed for. Therefore the usage of POMs as a floating gate offers two alternatives. First, if chemical synthesis in combination with self-assembly or controlled deposition can yield a nearly perfect monolayer of POMs, a multi-bit memory cell is possible. Alternatively, the multiple reducibility of the POMs offers a safeguard against variability in the configuration of the floating gate, allowing the desired net stored charge density to be achieved even if perfect regularity of the POM layer is not achievable.

Atomic-level DFT simulation approaches provide a deep insight into the structure and electronic properties of polyoxometalates. At the same time, device modelling at a mesoscopic level has proven to be an indispensable tool in the design and optimisation of novel devices, especially when account for the statistical variability at the nanoscale is vital. The synergy of the two approaches exploited in our work allowed us to theoretically evaluate a novel memory cell device incorporating POMs. Presently, substantial efforts are devoted to the extension of the hierarchical modelling framework to allow transport calculation through the tunnelling oxide, with the aim of evaluating the programming and retention capabilities of a device with a POM-floating gate. Our final aim is to provide informed guidance for both chemical synthesis and device design and fabrication, with the knowledge derived from device modelling and DFT calculations to yield real candidate flash-RAMs using complementary metal oxide semiconductor (CMOS) technology but incorporating polyoxometalate "molecular technology". This raises the very real prospect that polyoxometalate clusters with carefully designed redox properties may not only become candidates for incorporation into commercial flash-RAM, but also may set a new agenda for the design of non-volatile molecular memory systems that approach the molecular or atomic limit in years to come.

## Modelling Details

**Computational methodology:** Calculations were carried out using DFT methodology with the ADF 2008 program.<sup>[54]</sup> The exchange-correlation functionals of Becke and Perdew were used.<sup>[55]</sup> Relativistic corrections were included by means of the ZORA formalism. Triple- $\zeta$  polarisation basis sets were employed to describe the valence electrons of W, Mo, O, and S. All the structures were optimised in the presence of a continuous model solvent by means of the conductor-like screening model (COSMO). See the Supporting Information for more details on the computational settings.

**Device simulation methodology:** The 3D numerical simulations of the flash-cell performed with the commercial simulator GARAND, which deploys the drift-diffusion transport formalism and includes quantum corrections by means of the density-gradient approach.<sup>[22]</sup> Quantum corrections are essential for the accurate modelling of decananometre devi-

ces.<sup>[39]</sup> The capabilities of the simulator are extended to allow the incorporation of arbitrary fixed charge distribution in the gate oxide, to model the storage media of the flash-memory cell. See the Supporting Information for more details on the methodology.

## Acknowledgements

This work was supported by the ESPRC (Molecular-Metal-Oxide-nanoelectronicS (M-MOS): Achieving the Molecular Limit Ref: EP/H024107/1), The University of Glasgow, WestCHEM, the Leverhulme Trust and the Royal Society/Wolfson Foundation. We would like to express our gratitude to The Quantum Chemistry Group of the Universitat Rovira i Virgili (URV), Tarragona, for computational resources. We wish to acknowledge Dr. Xavier López for fruitful discussion and valuable suggestions made during the preparation of this work.

- [1] a) L. C. W. Baker, D. C. Glick, *Chem. Rev.* **1998**, *98*, 3–49; b) M. T. Pope in *Heteropoly and Isopoly Oxometalates*, Springer, Berlin, **1983**; c) P. Souchay in *Polyanions et Polycations*, Gauthier-Villars, Paris, **1963**.
- [2] J. Berzelius, *Poggendorf's Ann. Phys.* **1826**, *82*, 369.
- [3] C. Marignac, *Ann. Chim. Phys.* **1864**, *3*, 1.
- [4] M. T. Pope, A. Müller in *Polyoxometalates: from Platonic Solids to Anti-Retroviral Activity*, Kluwer, Dordrecht, **1994**; pp. 255–408.
- [5] a) J. E. Toth, F. C. Anson, *J. Am. Chem. Soc.* **1989**, *111*, 2444–2451; b) J. E. Toth, J. D. Melton, D. Cabelli, B. H. J. Bielski, F. C. Anson, *Inorg. Chem.* **1990**, *29*, 1952–1957.
- [6] a) I. A. Weinstock, R. H. Atalla, R. S. Reiner, M. A. Moen, K. E. Hammel, C. J. Houtman, C. L. Hill, *New J. Chem.* **1996**, *20*, 269–275; b) I. A. Weinstock, R. H. Atalla, R. S. Reiner, M. A. Moen, K. E. Hammel, C. J. Houtman, C. L. Hill, *J. Mol. Catal. A* **1997**, *116*, 59–84.
- [7] a) E. Papaconstantinou, *Chem. Soc. Rev.* **1989**, *18*, 1–31; b) A. Mylonas, E. Papaconstantinou, *J. Mol. Catal.* **1994**, *92*, 261–267; c) E. Papaconstantinou, A. Ioannidis, A. Hiskia, P. Argitis, D. Dimotikali, S. Korres in *Polyoxometalates: from Platonic Solids to Anti-Retroviral Activity* (Eds. M. T. Pope, A. Müller), Kluwer, Dordrecht **1994**, pp. 327–336; d) C. M. Prosser-McCarthy, C. L. Hill, *J. Am. Chem. Soc.* **1990**, *112*, 3671–3673; e) J. F. W. Keana, M. D. Ogan, Y. Lu, M. Beer, J. Varkey, *J. Am. Chem. Soc.* **1985**, *107*, 6714–6715; f) J. F. W. Keana, *J. Am. Chem. Soc.* **1986**, *108*, 7951–7957.
- [8] a) C. L. Hill, D. A. Bouchard, *J. Am. Chem. Soc.* **1985**, *107*, 5148–5157; b) C. L. Hill, D. A. Bouchard, M. Kadkhodayan, M. M. Williamson, J. A. Schmidt, E. F. Hilinski, *J. Am. Chem. Soc.* **1988**, *110*, 5471–5479; c) M. A. Fox, R. Cardona, E. Gaillardet, *J. Am. Chem. Soc.* **1987**, *109*, 6347–6354; d) R. C. Chambers, C. L. Hill, *Inorg. Chem.* **1991**, *30*, 2776–2781; e) A. Hiskia, E. Papaconstantinou, *Inorg. Chem.* **1992**, *31*, 163–167.
- [9] a) J. M. Clemente-Juan, E. Coronado, *Coord. Chem. Rev.* **1999**, *193*, 361–394; b) D.-L. Long, R. Tsunashima, L. Cronin, *Angew. Chem.* **2010**, *122*, 1780–1803; *Angew. Chem. Int. Ed.* **2010**, *49*, 1736–1758.
- [10] a) J. Lehmann, A. Gaita-Arino, E. Coronado, D. Loss, *Nat. Nanotechnol.* **2007**, *2*, 312; b) M. A. Aldamen, J. M. Clemente-Juan, E. Coronado, C. Marti-Gastaldo, A. Gaita-Arino, *J. Am. Chem. Soc.* **2008**, *130*, 8874; c) J. M. Clemente-Juan, E. Coronado, A. Gaita-Arino, *Chem. Soc. Rev.* **2012**, *41*, 7464–7478.
- [11] a) A. F. Wells in *Structural Inorganic Chemistry*, Oxford University Press, Oxford, 1st ed., **1945**, pp. 344; b) B. Dawson, *Acta Crystallogr. Sect. B* **1953**, *6*, 113–126; c) R. Strandberg, *Acta Chem. Scand. Ser. A* **1975**, *29a*, 350–358; d) R. Acerete, C. Hammer, L. C. Baker, *Inorg. Chem.* **1984**, *23*, 1478–1484; e) H. Ichida, Y. Sasaki, *Acta Crystallogr. Sect. C. Cryst. Struct. Commun.* **1983**, *39*, 529–533; f) R. Contant, R. Thouvenot, *Inorg. Chim. Acta* **1993**, *212*, 41–50.
- [12] N. Fay, A. M. Bond, C. Baffert, J. F. Boas, J. R. Pillbrow, D.-L. Long, L. Cronin, *Inorg. Chem.* **2007**, *46*, 3502–3510.
- [13] C. Fleming, D.-L. Long, N. McMillan, J. Johnson, N. Bovet, V. Dhanak, N. Gadegaard, P. Kögerler, L. Cronin, M. Kadodwala, *Nat. Nanotechnol.* **2008**, *3*, 229–233.
- [14] a) Y. Ozawa, Y. Sasaki, *Chem. Lett.* **1987**, 923–926; b) Y. Jeannin, J. Martin-Frere, *Inorg. Chem.* **1979**, *18*, 3010–3014; c) S. Himeno, A. Saito, T. Hori, *Bull. Chem. Soc. Jpn.* **1990**, *63*, 1602–1606; d) U. Kortz, M. T. Pope, *Inorg. Chem.* **1994**, *33*, 5643–5646.
- [15] a) C. Baffert, S. W. Feldberg, A. M. Bond, D. L. Long, L. Cronin, *Dalton Trans.* **2007**, 4599–4607; b) D.-L. Long, H. Abbas, P. Kögerler, L. Cronin, *Angew. Chem.* **2005**, *117*, 3481–3485; *Angew. Chem. Int. Ed.* **2005**, *44*, 3415–3419.
- [16] J. Yan, D.-L. Long, E. F. Wilson, L. Cronin, *Angew. Chem.* **2009**, *121*, 4440–4444; *Angew. Chem. Int. Ed.* **2009**, *48*, 4376–4380.
- [17] D.-L. Long, Y. F. Song, E. F. Wilson, P. Kögerler, S. X. Guo, A. M. Bond, J. S. J. Hargreaves, L. Cronin, *Angew. Chem.* **2008**, *120*, 4456–4459; *Angew. Chem. Int. Ed.* **2008**, *47*, 4384–4387.
- [18] a) D.-L. Long, P. Kögerler, A. D. C. Parenty, J. Fielden, L. Cronin, *Angew. Chem.* **2006**, *118*, 4916–4921; *Angew. Chem. Int. Ed.* **2006**, *45*, 4798–4803; ; b) C. Ritchie, E. M. Burkholder, D.-L. Long, D. Adam, P. Kögerler, L. Cronin, *Chem. Commun.* **2007**, 468–470.
- [19] P. A. Lewis, C. E. Inman, F. Maya, J. M. Tour, J. E. Hutchison, P. S. Weiss, *J. Am. Chem. Soc.* **2005**, *127*, 17421–17426.
- [20] A. Aviram, M. Eatner, *Chem. Phys. Lett.* **1974**, *29*, 277.
- [21] J. E. Green, J. W. Choi, A. Boukai, Y. Bunimovich, E. Johnston-Halperin, E. DeIonno, Y. Luo, B. A. Sheriff, K. Xu, Y. S. Shin, H.-R. Tseng, J. F. Stoddart, J. R. Heath, *Nature* **2007**, *445*, 414–417.
- [22] Gold Standard Simulations Limited (GSS Ltd.), The University of Glasgow, Glasgow, UK (<http://www.GoldStandardSimulations.com>).
- [23] D.-L. Long, L. Cronin, *Chem. Eur. J.* **2006**, *12*, 3698–3706.
- [24] a) M. White, Y. Yang, A. Purwar, M. French, *IEEE Trans. Comp. Packaging Manufacturing Tech. - Part A* **1998**, *20/2*, 190–195; b) J. Lee, S. H. Hur, J.-D. Choi, *IEEE Electron Device Lett.* **2002**, *23/5*, 264–266.
- [25] C.-Y. Lu, K.-Y. Hsieh, R. Liu, *Microelectron. Eng.* **2008**, *86*, 283–286.
- [26] S. Tiwari, F. Rana, K. Chan, H. Hanafi, W. Chan, D. Buchanan, *IEEE Intl. Electron Devices Meeting* **1995**, 521–524.
- [27] B. Kumar, P. R. Nair, R. Sharma, S. Kamohara, S. Mahapatra, *IEEE Trans. Electron Devices* **2006**, *53/4*, 698–705.
- [28] J. Shaw, T.-H. Hou, H. Raza, E. Kan, *IEEE Trans. Electron Devices* **2009**, *56/8*, 1729–1735.
- [29] T. Pro, J. Buckley, K. Huang, A. Calborean, M. Gely, G. Delapierre, G. Ghibauda, F. Duclairoir, J.-C. Marchon, E. Jalaguier, P. Maldivi, B. De Salvo, S. Deleonibus, *IEEE Trans. Nanotechnol.* **2009**, *8/2*, 204–213.
- [30] J. Shaw, Y.-W. Zhong, K. Hughes, T.-H. Hou, H. Raza, S. Rajawade, J. Bellfy, J. R. Engstrom, H. D. Abruna, E. Kan, *IEEE Trans. Electron Devices* **2011**, *58/3*, 826–834.
- [31] C. Musumeci, M. H. Rosnes, F. Giannazzo, M. D. Symes, L. Cronin, B. Pignataro, *ACS Nano* **2011**, *5*, 9992–9999.
- [32] J. A. Fernández, X. López, C. Bo, C. de Graaf, E. J. Baerends, J. M. Poblet, *J. Am. Chem. Soc.* **2007**, *129*, 12244–12253.
- [33] X. López, C. Bo, J. M. Poblet, *Chem. Soc. Rev.* **2003**, *32*, 297–308.
- [34] X. López, C. Bo, J. M. Poblet, *J. Am. Chem. Soc.* **2002**, *124*, 12574–12582.
- [35] A. W. A. Mariotti, J. Xie, B. F. Abrahams, A. M. Bond, A. G. Wedd, *Inorg. Chem.* **2007**, *46*, 2530–2540.
- [36] J. Xie, B. F. Abrahams, A. G. Wedd, *Chem. Commun.* **2008**, 576–578.
- [37] D. L. Long, P. Kögerler, L. Cronin, *Angew. Chem.* **2004**, *116*, 1853–1856; *Angew. Chem. Int. Ed.* **2004**, *43*, 1817–1820.
- [38] J. Zhang, A. M. Bond, P. J. S. Richardt, A. G. Wedd, *Inorg. Chem.* **2004**, *43*, 8263–8271.
- [39] A. Asenov, G. Slavcheva, A. R. Brown, J. Davies, S. Saini, *IEEE Trans. Electron Devices* **2001**, *48/4*, 722–729.
- [40] D. M. Way, J. B. Cooper, M. Sadek, T. Vu, P. J. Mahon, A. M. Bond, R. T. C. Brownlee, A. G. Wedd, *Inorg. Chem.* **1997**, *36*, 4227–4233.

- [41] B. Carole, S. W. Feldberg, A. M. Bond, D. L. Long, L. Cronin, *Dalton Trans.* **2007**, 4599–4607.
- [42] X. López, J. M. Maestre, C. Bo, J. M. Poblet, *J. Am. Chem. Soc.* **2001**, *123*, 9571–9576.
- [43] L. Yan, X. López, J. J. Carbó, R. T. Sniatynsky, D. D. Duncan, J. M. Poblet, *J. Am. Chem. Soc.* **2008**, *130*, 8223–8233.
- [44] I.-M. Mbomekallé, X. López, J. M. Poblet, F. Sécheresse, B. Keita, L. Nadjo, *Inorg. Chem.* **2010**, *49*, 7001–7006.
- [45] I.-M. Mbomekallé, X. López, J. M. Poblet, F. Sécheresse, B. Keita, L. Nadjo, *Inorg. Chem.* **2010**, *49*, 7001–7006.
- [46] A. Lewis, J. A. Bumpus, D. G. Truhlar, C. J. Cramer, *J. Chem. Educ.* **2004**, *81*, 596–604.
- [47] S. Markov, X. Wang, N. Moezi, A. Asenov, *IEEE Trans. Electron Devices* **2011**, *58/8*, 2385–2393.
- [48] S. M. Amoroso, A. Maconi, A. Mauri, C. M. Compagnoni, A. Spinelli, A. Lacaíta, *IEEE Trans. Electron Devices* **2011**, *58/7*, 1864–1871.
- [49] M. Kim, S. D. Chae, H. S. Chae, J. H. Kim, Y. S. Jeong, *IEEE Trans. Nanotechnol.* **2004**, *3/4*, 417–425.
- [50] M. Swart, P. Th. van Duijnen, J. G. Snijders, *J. Comput. Chem.* **2001**, *22*, 79–88.
- [51] A. S. Grove, *Physics and Technology of Semiconductor Devices*, Wiley, New York, **1967**.
- [52] K.-D. Suh, B.-H. Suh, Y.-H. Lim, J.-K. Kim, Y.-J. Choi, Y.-N. Koh, S.-S. Lee, S.-C. Kwon, B.-S. Choi, J.-S. Yum, J.-H. Choi, J.-R. Kim, H.-K. Lim, *IEEE J. Solid-State Circuits* **1995**, *30/11*, 1149–1156.
- [53] A. Asenov, A. R. Brown, J. H. Davies, S. Kaya, G. Slavcheva, *IEEE Trans. Electron Devices* **2003**, *50*, 1837–1852.
- [54] a) ADF 2008. 01, SCM, Theoretical Chemistry, Vrije Universiteit, Amsterdam, The Netherlands (<http://www.scm.com>); b) G. te Velde, F. M. Bickelhaupt, S. J. A. van Gisbergen, C. Fonseca Guerra, E. J. Baerends, J. G. Snijders, T. Ziegler, *J. Comput. Chem.* **2001**, *22*, 931–967.
- [55] a) A. D. Becke, *J. Chem. Phys.* **1986**, *84*, 4524–4529; b) A. D. Becke, *Phys. Rev. A* **1988**, *38*, 3098–3100; c) J. P. Perdew, *Phys. Rev. B* **1986**, *33*, 8822–8824; d) J. P. Perdew, *Phys. Rev. B* **1986**, *34*, 7406–7406.

Published online: November 8, 2013